

Contents

G. Hoffmann et <i>al.</i> / Tunnelling induced fluorescence as a probe of electromagnetic interaction at nanometre proximity	2
--	---

TUNNELLING INDUCED FLUORESCENCE AS A PROBE OF ELECTROMAGNETIC INTERACTION AT NANOMETRE PROXIMITY

GERMAR HOFFMANN

*Institut für Experimentelle und Angewandte Physik,
Christian-Albrechts-Universität zu Kiel,
D-24098 Kiel, Germany*

JAVIER AIZPURUA

*National Institute of Standards and Technology,
Gaithersburg, Maryland 20899-8423, USA*

S. PETER APELL

*University Outreach, Kristianstad University,
SE-291 88 Kristianstad, Sweden*

RICHARD BERNDT

*Institut für Experimentelle und Angewandte Physik,
Christian-Albrechts-Universität zu Kiel,
D-24098 Kiel, Germany*

1. Abstract

Fluorescence induced by the tunnelling current of a scanning tunnelling microscope is used to investigate the electromagnetic coupling of a metal tip and a metal sample. Sub-atomic scale modifications of the tunnelling junction geometry cause spectral shifts of the fluorescence. Such shifts are observed when the tip is vertically displaced relative to a flat sample surface. Similarly, monatomic sample steps close to the tip position shift the fluorescence. These experimental results are consistent with model calculations of the electromagnetic response of an appropriate tip-sample geometry. We find that for sharp tips the electromagnetic coupling of the tip and the sample is confined to a lateral range of a few nm.

2. Introduction

The electromagnetic interaction of objects in nanometre proximity plays a central role in surface enhanced Raman scattering [1] and it is vital to scanning probe techniques such as non-contact atomic force microscopy [2] or scanning near-field optical microscopy [3]. In these microscopies, the electromagnetic coupling of the tip and a sample leads to the formation of new, localized electromagnetic modes. In the scanning tunnelling microscope (STM), these modes can be excited by inelastic electron tunnelling and give rise to the emission of characteristic fluorescence [4, 5, 6, 7, 8, 9]. Owing to the ability of the STM to precisely control the vertical and lateral position of the tip spectral analysis of this fluorescence can be used to study the electromagnetic coupling on an atomic scale.

Here, we report on such experiments, first described in Ref. [10]. In the vicinity of a monoatomic step we observe gradual shifts of fluorescence spectra when crossing the step in lateral direction. Related shifts occur when the tip is retracted from an atomically flat metallic surface. These results are quantitatively compared to model calculation of the electromagnetic coupling where the tip is assumed to be a revolution hyperboloid with a radius of curvature of a few nm. From these analyses the lateral extension of the coupled surface plasmon mode, which is induced at the cavity by the proximity of the tip, is estimated. Understanding the implications of sub-atomic modifications of the cavity in these simple cases may give us a better approach for topographically more complex systems such as adsorbed molecules.

3. Instrumentation

The experiments were performed with a custom built STM in ultra-high vacuum (UHV) at low temperature (5 K). A lens system collects and transfers the light to a grating spectrometer and finally to a CCD camera [12]. Au and Ag (111)-surfaces as well as Au and Ag-covered W tips were prepared in UHV by standard Ar-ion sputtering and annealing cycles. Surface structures were verified before and after all experiments with STM to rule out surface modifications

4. Experimental observations

Figure 1b shows a fluorescence spectrum recorded from a defect-free Ag(111) surface at a distance of 55 Å from the next step. Circles indicate raw data, dots are corrected for the detection efficiency which is shown separately in Figure 1a. The acceptance angle, chromatic aberrations, reflectivities of

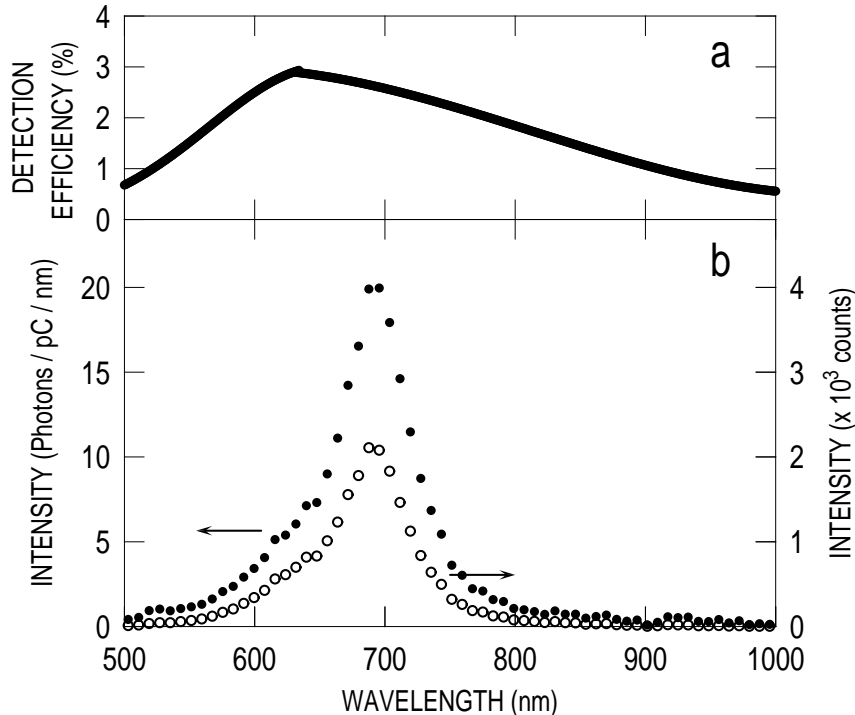


Figure 1. (a) Wavelength dependent detection efficiency of the optical setup. (b) Fluorescence spectrum of a flat Ag(111) surface and a Ag-covered W tip at a sample voltage $V = 2.9$ V and a tunnelling current $I = 5$ nA as measured in 0.1 seconds (circles) and corrected for the detection efficiency (dots).

the optical setup as well as the detection efficiency of the CCD camera are taken into account [15]. An intensity peak occurs at a wavelength $\lambda \approx 690$ nm with a broad tail to the short wavelength side. The spectrum is similar to previously reported and calculated spectra from Ag tips on Ag samples [6, 13]. It is due to the plasmon resonance for the given tip-sample distance and tip shape. We note that $V = 2.9$ V was chosen sufficiently large to have the peak fully developed.

At this point it is useful to introduce the definition of a mean emission wavelength $\bar{\lambda} = \int \lambda P(\lambda) d\lambda / (\int P(\lambda) d\lambda)$, where P is the spectral density of the measured fluorescence. Using this definition, the wavelength resolution of a shift is improved. This procedure is acceptable since the spectral shape does not change significantly over the range of distances probed here. Uncertainties due to counting statistics are indicated in the following graphs by error bars. The offset between the peak position and $\bar{\lambda}$ is ≈ -20 nm. The uncertainty of the peak position is the root mean square or combined standard uncertainty of the statistical uncertainty (less than ± 1 nm), and

the systematic uncertainty (± 4 nm).

Figure 2 shows experimental data recorded from a monoatomic step on Ag(111). This step was chosen to be straight over a distance of ≈ 300 Å. The solid line represents a cross-sectional profile of a constant current topograph. At each STM image point a fluorescence spectrum was recorded, similar to the data of Fig. 1. From the spectra overall shifts of the emission are observed while the spectral shape remains unaffected. In Figure 2b (dots) we evaluate the shift of the mean wavelength (relative to a spectrum on the flat terrace) versus the tip position. As the tip approaches the step from the upper atomic terrace, the emission shifts to shorter wavelength whereas a red-shift occurs when approaching from the lower terrace. The shifts are discernible up to a lateral distance of ≈ 50 Å from the step.

To understand this spectral shift it is useful to consider the lateral extension of the surface mode induced at the tip-sample cavity and the tip-sample distance d . The lowest-energy mode, which corresponds to charges of opposite signs on the boundaries, causes the light emission in STM [5]. For a vacuum gap of width d between a semi-infinite free-electron metal sample and a sharp tip this mode disperses according to $\hbar\omega \sim d^{1/n}$, where n depends on the particular geometry of the tip [17]. A surface step within the lateral range of the plasmon mode can be viewed as a variation of the effective distance d . When the tip is located on the upper terrace the distance between tip and sample averaged over the lateral extension of the plasmon is effectively increased yielding a blue-shift. When the tip approaches the step the tip-sample distance effectively increases further as well as the blue-shift. This shift of the emission peak is a consequence of the interaction of the surface mode with the step. Estimating the extension of the localized mode as the distance where the shift becomes noticeable we find a value of ≈ 50 Å. This value is consistent with previous model calculations for the extension of the mode at the cavity [16].

The above concept of an effective tip-sample d can be tested experimentally. To this end we varied d over a flat area of a Au(111) sample, i.e., in absence of any steps, and simultaneously recorded some 680 fluorescence spectra. The spectra are similar to previously reported spectra of this material combination [13, 18]. The integrated intensity vs. the current is plotted in Figure 3a. As expected, an exponential variation is found. Figure 3b displays the shift of mean emission wavelength $\bar{\lambda}$ versus the tunnelling current and the associated tip excursion. An approximately linear blue-shift of $\bar{\lambda}$ with the tip excursion Δd is observed with a slope of 3 nm/Å.

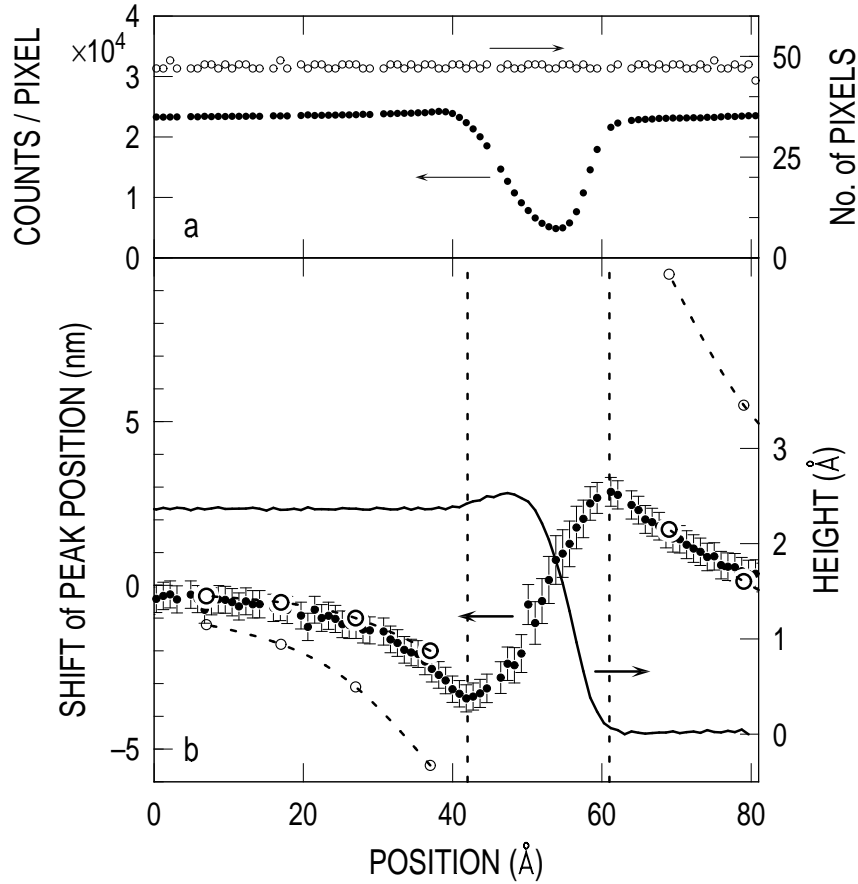


Figure 2. (a) Profile of the integrated intensity (dots) across a monoatomic Ag(111) step. To improve signal-to-noise ratio spectra from consecutive linescans recorded at identical distances from the step were integrated. Since the step was not exactly perpendicular to the scan direction each linescan is shifted by a fraction of pixel relative to the previous scan. Therefore, the average intensity at each data point and the number of pixels used per data point are indicated. Data points polluted by cosmic rays are removed. Directly at the step edge the intensity is reduced. (b) Cross-sectional profile of the constant current topograph (line), along with the shifts of the mean wavelength (dots with error bars) from fluorescence spectra recorded at each STM image point. Model calculations for an axially symmetric step (hole and island) are indicated by small circles ($\Delta\lambda_{\text{island}}$). Corrected values for a one dimensional step are plotted as large circles ($\Delta\lambda_{\text{step}}$). Vertical dashed lines delimit the immediate proximity of the step where significant vertical tip motion occurs.

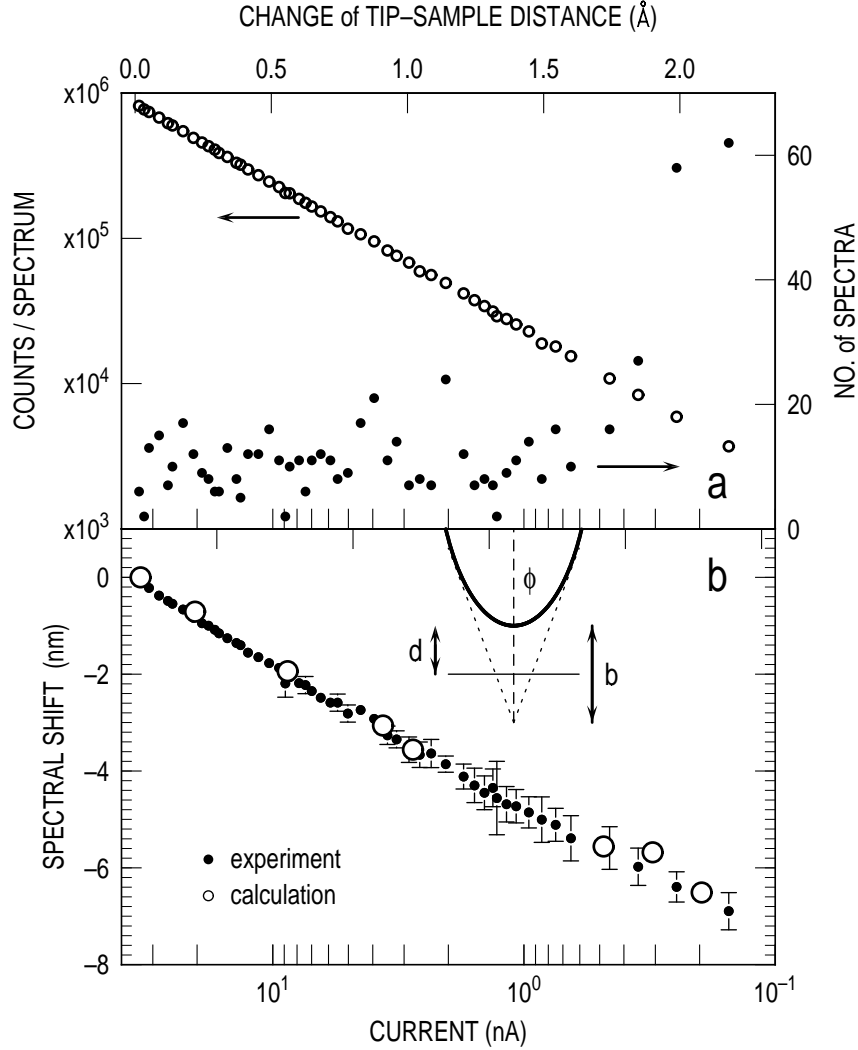


Figure 3. (a) Total intensity per spectrum vs. current (circles) and number of spectra used for averaging (dots). (b) Shift of mean emission wavelength $\bar{\lambda}$ vs. tunnelling current and associated vertical tip displacement, as measured (dots) and calculated (circles). The inset shows the tip geometry used for modelling the data.

5. Numerical Calculations

The experimental data can be analysed further by numerical model calculations within the model of Ref. [16]. In this model the tip is represented by a hyperboloid with an aperture angle ϕ and a tip apex parameter b located at a distance d above the flat surface (see inset in Fig. 3). The geometric

parameters ϕ and b of the tip correspond to a radius of curvature of the tip $R = b \tan(\phi)$. The light emission is calculated as an incoherent sum of the inelastic transitions of energy $\hbar\omega$ between tip and sample states at energies E_t and E_s which lead to the current density $\vec{j}_{ts}(\vec{r}^j, \omega)$, weighed by the field enhancement in the tip-sample gap $G(\vec{r}^j, \omega)$. In this model, the radiated power per photon energy and solid angle is:

$$\frac{d^2 P}{d\Omega d(\hbar\omega)} = \frac{\omega^2}{8\pi^2 \varepsilon_0 c^3} \sum_{t,s} \left| \int d^3 r^j G(\vec{r}^j, \omega) \vec{j}_{ts}(\vec{r}^j, \omega) \right|^2 \times \delta(E_t - E_s - \hbar\omega), \quad (1)$$

where c is the velocity of light. The field enhancement factor $G(\vec{r}^j, \omega)$ determines the electromagnetic modes at the cavity. It is determined with a boundary element method using bulk dielectric functions [19]. Tersoff and Hamann's model extended to high energy losses [16, 20] is used to calculate the tunnelling current.

The overall aperture of the tip ϕ mainly controls the position of the emission peak. Small changes of this parameter can lead to wavelength changes of several ten nm. The other geometrical parameters, the tip-sample separation distance d and the apex length parameter b , enable a fine tuning of the peak position. Moreover, b determines the shift of the peak with vertical tip excursion. We find shifts of $\approx 3 \text{ nm}/\text{\AA}$ for sharp tips ($R = 10 \text{ \AA}$) up to $\approx 10 \text{ nm}/\text{\AA}$ for blunt tips ($R > 150 \text{ \AA}$). In modelling a particular experiment, ϕ and b are first chosen to fit calculated spectra to the experimental data. Then d is varied as in the experiment. The resulting calculated shifts of the peak positions are shown in Fig. 3 (circles). The observed shifts are due to the geometry-controlled variation of the field enhancement $G(\vec{r}^j, \omega)$. A quantitative agreement with the experiment is achieved for sharp tip apex ($R = 10 \text{ \AA}$) along with a fairly wide aperture of the tip ($\phi = 40^\circ$).

From the above experimental and calculated results it is clear that the tip-sample separation d and the fluorescence spectrum are directly related. We now attempt to adapt the theoretical concept to the case of an atomic step. To reduce the numerical expense of the problem, in a first step, we preserve the axial symmetry by modelling the step as a hole (or island) with the tip placed in the center as indicated in Fig. 2a. Within this calculation different island (or hole) radii represent different distances from the step. Clearly, this geometry overestimates the influence of a step. This will be corrected for later on. Next, we restrict the calculations to the range where no topographical contrast in the linescan can be observed, i.e., outside of the close proximity of the step. Then we can safely assume that the energy dependent current density $\vec{j}_{ts}(\vec{r}^j, \omega)$ is constant and does

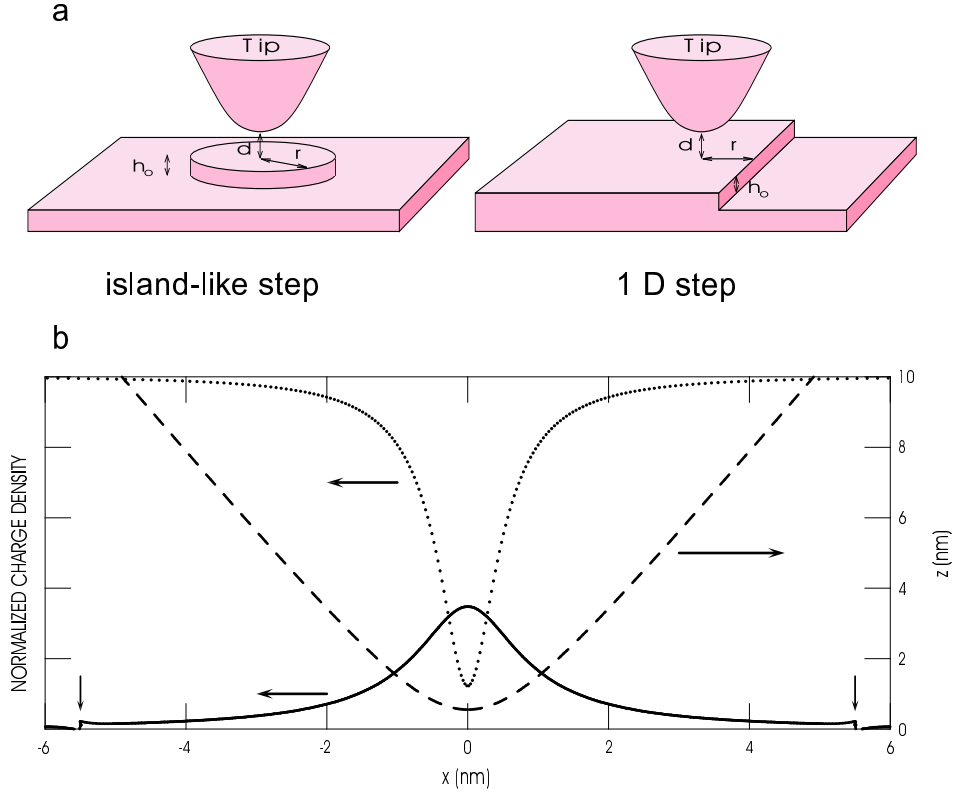


Figure 4. (a) Geometries used to model light emission near a step. Left: Step showing azimuthal symmetry to obtain Δ_{island} in Fig. 1. Right: One dimensional step used for obtaining the corrected Δ_{step} in Fig. 1. (b) Cross section of the tip-sample geometry (dashed line) and the calculated charge densities on the tip (dots) and sample (line) at a lateral tip-step distance of $\rho = 55 \text{ \AA}$.

not contribute to additional variations of the fluorescence. We note that quantitative modelling very close to the step would require information on the atomic tip structure and the precise electronic structure at the step. As in the experiment, the calculated spectral shape does not change as ρ is varied while there are overall shifts. These shifts are evaluated from the spectra and indicated by dots in Fig. 2. In agreement with the experiments we find a blue-shift when the tip is located on the top of an island (which corresponds to a tip position on an upper terrace) and a red-shift on the bottom of a hole (corresponding to the tip on a lower terrace).

Fig. 4b shows the calculated charge densities of the mode relevant for light emission and the tip geometry. Owing to the tip curvature the mode is localized. We define the extension of electromagnetic coupling to be the spatial extent of the induced surface plasmon on the sample side. For a

tip with radius $R = 10 \text{ \AA}$, we find a lateral extension of only $\approx 20 \text{ \AA}$ as determined by the full width at half maximum of the plasmon charge density. Note, however, that the tail of the plasmon mode extends up to more than twice this value, as shown in Fig. 4b. At this distance the presence of the step only causes a minor redistribution of the charge density (indicated by two vertical arrows). The localized mode at the sample surface suffers a stronger modification when the center of the mode (which is identical to the tip position) is closer to the monoatomic step. The lateral distance where the shift becomes discernible is connected with the range of the interaction of the plasmon mode with the step. In the present case, the experimental extension is $\approx 50 \text{ \AA}$ which agrees with the model calculations for the sharp tips used in Fig. 4b.

As expected, the calculated shifts from the axially symmetric model are larger than the experimental data. Above it was shown that a change Δd of the tip-sample distance leads to a linear shift of the spectral maximum: $\Delta\lambda \sim \Delta d$. A variation of the surface height $h(\vec{r})$ within the lateral range of the plasmon mode will effectively change the average tip-sample distance. Therefore, we define an effective distance $d_{\text{eff}} = d + \Delta d_{\text{eff}}$ where

$$\Delta d_{\text{eff}} = \int \sigma_s(\vec{r}) h(\vec{r}) d^2\vec{r}. \quad (2)$$

σ_s is the normalized ($\int \sigma_s(\vec{r}) d^2\vec{r} = 1$) charge density of the plasmon mode on the sample surface as calculated. This convolution of height change and surface charge density accounts for any surface variation over the area where the surface plasmon extends. For a hole (or island), $h = 0$ within a circle of radius ρ , and $h = \pm h_0$ outside (see left side of Fig. 4). Similarly, for the case of a one-dimensional ascending or descending step at $x = \rho$, we have $h = \pm h_0$ for $x > \rho$ and $h = 0$ elsewhere (right of Fig. 4). The shift $\Delta\lambda_{\text{island}}$ originally calculated for the case of an axially symmetric step is then corrected by the convolution with the more realistic geometry:

$$\Delta\lambda_{\text{step}} = \frac{\Delta d_{\text{step}}}{\Delta d_{\text{island}}} \Delta\lambda_{\text{island}}. \quad (3)$$

The resulting data (squares in Fig. 2) are close to the measured spectral shifts. We note that the presence of a second descending step at the position 125 \AA is also taken into account in calculating $\Delta\lambda_{\text{step}}$.

6. Molecular Systems

The role of an organic molecules on metal surfaces in light emission has repeatedly been investigated [21, 22, 23, 24, 25]. While molecular-scale contrast was observed in maps of the photon intensity, for the systems

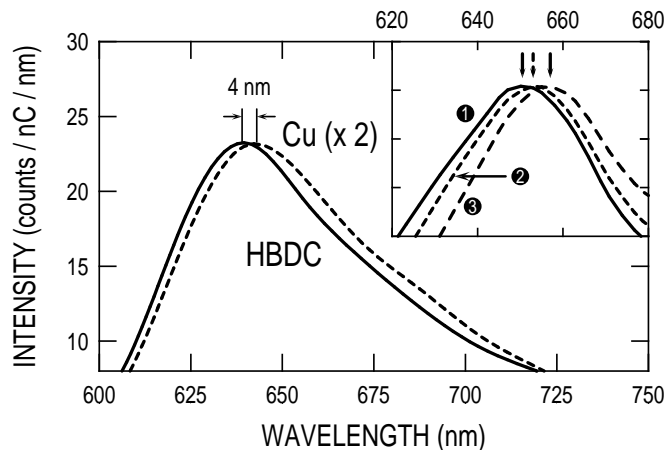


Figure 5. Fluorescence spectra from HBDC and the surrounding metal surface acquired with a W tip ($I = 5$ nA, $V = 2.3$ V). Spectra are scaled to same maximum intensity. They reveal a blue shift of the emission on HBDC. The inset shows three spectra from Au(111) recorded at different currents, i.e., different tip-sample distances. Spectrum (1) was recorded at $V = 3$ V and $I = 0.3$ nA. Spectrum (2) at $I = 2.8$ nA is red-shifted by $\Delta\lambda = 2$ nm, spectrum (3) at $I = 33.7$ nA is shifted further with $\Delta\lambda = 6$ nm.

studied to date, no compelling evidence of molecular fluorescence has been obtained. A recent example is the organic molecule HBDC (hexa-tert.-butyl-decacyclene) adsorbed on Cu(111). HBDC, which appears as a ≈ 2 Å protrusion in STM images and causes prominent contrasts in photon maps on a sub-molecular scale [11]. Fluorescence spectra recorded on top of individual molecules and for comparison on the bare Cu(111) substrate are shown in Fig. 5. Except for a ≈ 4 nm red-shift of the fluorescence spectra on top of molecules the emission spectrum remain nearly unaffected. This is clear indication that the emission process is unchanged. For illustration the inset of Fig. 5 shows results from clean Au(111) where the tip-sample distance was varied. In both cases virtually identical characteristics are observed. When the tip is forced to retract from the metal substrate either by changing the set tunnelling current (inset) or by the presence of a molecule, the fluorescence is blue-shifted by similar amounts.

We are delighted to thank A. Baratoff for discussions. This work has been supported by the European Commission via the TMR network EMIT and the Deutsche Forschungsgemeinschaft.

References

1. *Surface Plasmons*, H. Raether (Springer Tracts in Modern Physics 111, Berlin 1988) and *Optical properties of Metal Clusters*, U. Kreibitz and M. Vollmer (Springer Series in Materials Science 25, Berlin 1995).
2. H.-J. Güntherodt, D. Anselmetti, E. Meyer (Eds.), *Forces in Scanning Probe Methods*, NATO ASI Series E, Vol. **286** (Kluwer, Dordrecht, 1995).
3. D. W. Pohl and D. Courjon (eds.), *Near Field Optics*, NATO ASI Series E, Vol. **241** (Kluwer, Dordrecht, 1993).
4. J. K. Gimzewski, J. K. Sass, R. R. Schlittler, J. Schott, Europhys. Lett. **8**, 435 (1989).
5. P. Johansson, R. Monreal, S. P. Apell, Phys. Rev. B **42**, 9210 (1990).
6. R. Berndt, J. K. Gimzewski, P. Johansson, Phys. Rev. Lett. **67**, 3796 (1991).
7. B. N. J. Persson and A. Baratoff, Phys. Rev. Lett. **68**, 3224 (1992).
8. M. Tsukada, T. Shimizu, K. Kobayashi, Ultramicroscopy **42-44**, 360 (1992).
9. S. Ushioda, Y. Uehara, M. Kuwahara, Appl. Surf. Sci. **60/61**, 448 (1992).
10. J. Aizpurua, G. Hoffmann, S. P. Apell, R. Berndt, Phys. Rev. Lett. **89**, 156803 (2002).
11. G. Hoffmann, L. Libioulle, R. Berndt, Phys. Rev. B, **65**, 212107 (2002).
12. G. Hoffmann, J. Kröger, R. Berndt, Rev. Sci. Instrum. **73**, 305 (2002).
13. R. Berndt, J. K. Gimzewski, P. Johansson, Phys. Rev. Lett. **71**, 3493 (1993).
14. R. Berndt and J. K. Gimzewski, Phys. Rev. B **48** 4746 (1993); V. Sivel, R. Coratger, F. Ajustron, J. Beauvillain, Phys. Rev. B **50** 5628 (1994).
15. We use 'counts' to indicate the number of detected photons while 'photons' refers to the estimated number of emitted photons, i.e., the data is corrected for the detection efficiency.
16. J. Aizpurua, S. P. Apell, R. Berndt, Phys. Rev. B **62**, 2065 (2000).
17. R.W. Rendell, D.J. Scalapino, B. Mühlischlegel, Phys. Rev. Lett. **41**, 1746 (1978).
18. R. Péchou *et al.*, J. Phys. III **6**, 1441 (1996).
19. *Handbook of Optical Dielectric Constants of Solids*, D. Palik (ed.) (Naval Research Laboratory, Washington D.C., 1985).
20. K. Stokbro, U. Quaade, F. Grey, Appl. Phys. A: Mater. Sci. Process. **66**, S907 (1998).
21. R. Berndt *et al.*, Science **262**, 1425 (1993).
22. I. I. Smolyaninov, Surf. Sci. **364**, 79 (1996).
23. S. Evoy, F. D. Pardo, P. M. S. John, H. G. Craighead, J. Vac. Sci. Technol. A **15**, 1438 (1997).
24. D. Fujita *et al.*, Surf. Sci. **454-456**, 1021 (2000).
25. G. E. Poirier, Phys. Rev. Lett. **86**, 83 (2001).